Self-Assembly of Escin Molecules at the Air−Water Interface as Studied by Molecular Dynamics
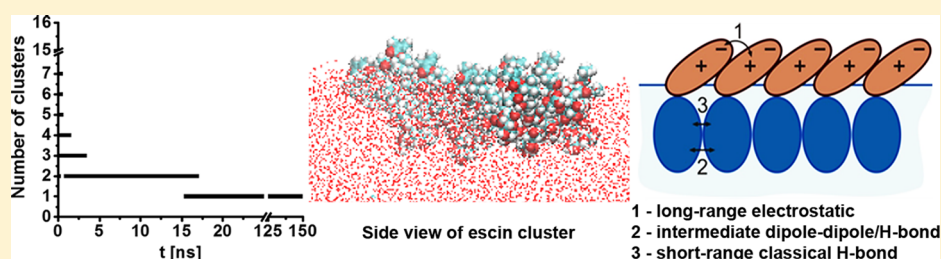
Sonya Tsibranska,[†] Anela Ivanova,*[,‡] Slavka Tcholakova,[†] and Nikolai Denkov[†]

[†]Department of Chemical and Pharmaceutical Engineering and [‡]Department of Physical Chemistry, Faculty of Chemistry and Pharmacy, University of Sofia, 1 James Bourchier Avenue, 1164 Sofia, Bulgaria

S *Supporting Information*

1 - long-range electrostatic
2 - intermediate dipole-dipole/H-bond
3 - short-range classical H-bond

ABSTRACT: Escin belongs to a large class of natural biosurfactants, called saponins, that are present in more than 500 plant species. Saponins are applied in the pharmaceutical, cosmetics, and food and beverage industries due to their variously expressed bioactivity and surface activity. In particular, escin adsorption layers at the air−water interface exhibit an unusually high surface elastic modulus (>1100 mN/m) and a high surface viscosity (ca. 130 N·s/m). The molecular origin of these unusual surface rheological properties is still unclear. We performed classical atomistic dynamics simulations of adsorbed neutral and ionized escin molecules to clarify their orientation and interactions on the water surface. The orientation and position of the escin molecules with respect to the interface, the intermolecular interactions, and the kinetics of molecular aggregation into surface clusters are characterized in detail. Significant differences in the behavior of the neutral and the charged escin molecules are observed. The neutral escin rapidly assembles in a compact and stable surface cluster. This process is explained by the action of long-range attraction between the hydrophobic aglycones, combined with intermediate dipole−dipole attraction and short-range hydrogen bonds between the sugar residues in escin molecules. The same interactions are expected to control the viscoelastic properties of escin adsorption layers.

INTRODUCTION

Saponins present a class of natural amphiphilic molecules that contain a hydrophobic scaffold (called aglycone) and one to several hydrophilic oligosaccharide chains connected to the aglycone via glucoside bonds. Some saponins are used as essential components in vaccine adjuvants, whereas others exhibit anti-inflammatory, antimicrobial, antiallergic, antivirus, cytotoxic, diuretic, hemolytic, and hypocholesterolemic activity.[1−5] The practical applications of saponins also include foam and emulsion stabilization in food, beverage, and cosmetic products, cholesterol removal from foods (fats, milk, etc.), and micellar solubilization of vitamins and minerals in food additives.[6−11]

To clarify the origin of various effects observed for saponin-containing systems and to optimize the applications of the latter, a better understanding is needed for the relationship between the molecular structure, on the one hand, and the structure and properties of their micellar aggregates and adsorption layers, on the other hand.[12,13] Such an understanding can be significantly improved using the method of molecular dynamics (MD).

Escin is the main natural constituent of the saponin extract from the seeds of *Aesculus hippocastanum* (known also as the horse chestnut tree).[14] Efficient methods allow escin isolation and purification as a single molecular component,[15] and it is sold as a market product. A number of bioactivity expressions of this saponin are detected, such as anti-inflammatory and blood vessel contracting and protecting properties.[1] Horse chestnut seed extract, containing around 20 wt % escin, is used in medicine for its venotonic effect, vascular protection, anti-inflammatory property, and free radical scavenging properties.

This compound is also a surfactant with some unusual adsorption characteristics. Escin adsorption layers feature an extremely high surface elastic modulus and very low gas permittivity, which is important to the properties of foams and emulsions stabilized by this natural surfactant.[12,13] These properties are sensitive to the pH of the water phase because the sugar residue, attached to the aglycone, contains an ionizable carboxyl group (Figure 1). For example, the surface elasticity decreases significantly upon pH increase; i.e., the adsorption layer formed from ionized escin molecules is less elastic than that composed of neutral ones.[12] The origin of this
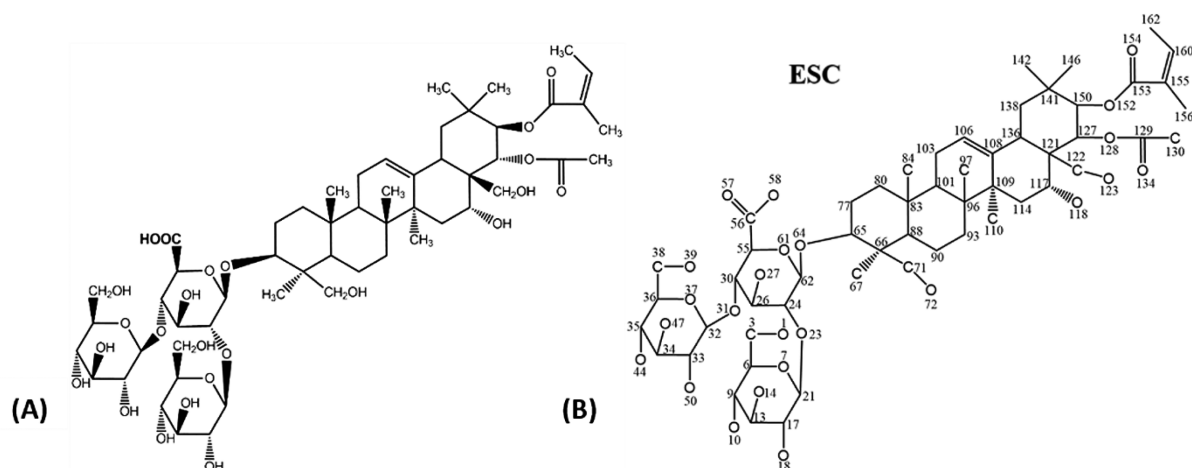
Figure 1. (A) Chemical formula of escin with cyclic hydrogens omitted for clarity. The carboxyl group containing a proton, which is removed in the anionic form, is denoted in bold. (B) Atom numbering of the non-hydrogen atoms in escin.

unusual surface behavior has not been clarified at the molecular level. Hence, escin is a bio- and surface-active substance that deserves to be studied in more depth, given its multiple potential applications.

Several publications report MD simulations of saponin molecules.[16−18] However, this group of papers is focused mainly on the kinetics, self-assembly mechanism, and shape of micelles formed in bulk saponin solutions. In the studies by Pedebos et al.,[16,17] the stable conformations of two types of saponins in aqueous and in pyridine solutions are determined by unrestrained MD and are shown to match NOESY NMR measurements well. One of these studies[17] reports for the first time the structure and conformation in aqueous solution of saponin QS-21, extracted from the *Quillaja saponaria* tree. This saponin is of particular interest because it is used as an essential component in the most efficient saponin-based vaccine adjuvants. A 3D atomistic model of QS-21, obtained by MD simulations, is proposed in the same study.[17] The MD modeling is combined with SAXS data to decipher the molecular conformation of QS-21 in the micelles and the forces leading to micellar growth upon concentration increase. In a separate study, Dai et al.[18] employ meso-MD and coarse-grained MD to discriminate the solubilization mechanisms of saikosaponin and ginsenoside Ro (bioactive compound in ginseng). The molecules of ginsenoside Ro form vesicles that, at low concentrations of saikosaponin, solubilize it in their surface layer, whereas mixed vesicles are obtained at higher saikosaponin concentrations.

Other works[19,20] report the results from MD simulations aimed at determining the populated conformations of saponins in solution and finding relationships between the molecular structure and certain bioactivity. Walkowicz et al.[19] study saponin QS-21 and a series of its synthetic analogues and establish a crucial role of the conformation of the central glycosydic bond with the adjuvant activity. Lin and Wang[20] employ atomistic and coarse-grained MD to study the conformations of dioscin in water, decane, and water−decane, its interaction with cholesterol, and its aggregation inside a lipid bilayer. On the basis of that, they propose a molecular mechanism for the hemolytic activity of this saponin that consists of two steps: initial penetration of the saponin in the membrane and strong binding to cholesterol, followed by

concentration-dependent curving of the membrane, subsequently leading to its destruction.

The MD method is also suitable for the interpretation of the rheological characteristics of surfactant adsorption layers at interfaces, which is demonstrated in the example of system 1,2-ethanebis(dimethyl dodecyl ammonium bromide-$C_{12}C_2C_{12}\cdot 2Br$) at the air/water interface.[21] It is determined experimentally that the dilatational modulus of $C_{12}C_2C_{12}\cdot 2Br$ is higher than that of DTAB (dodecyltrimethylammonium bromide), which is related to an interfacial force acting to compensate for the external perturbation of the adsorption layer. The authors explain this effect by MD simulations, which show that the difference between the dilatational moduli of the two types of surfactants is due to the higher concentration of Br^- counterions in the vicinity of the nitrogen atoms of $C_{12}C_2C_{12}\cdot 2Br$ than around those of DTAB. These ions reduce the repulsion between the hydrophilic groups and enhance the adsorption of $C_{12}C_2C_{12}\cdot 2Br$ at the interface.

This literature overview shows that there are no data from MD simulations of saponin adsorption layers. Hence, a theoretical study in this direction would provide new insights into the behavior of these peculiar molecular systems. The current work presents a detailed classical atomistic MD description of the properties of escin molecules (single and in a cluster) adsorbed at the vacuum−water interface. The main goal is to elucidate the molecular characteristics and the intermolecular interactions for the neutral (ESC) and for the anionic (ESCA) forms of this saponin. A relation to the aforementioned rheological properties of the escin adsorption layers is also sought.

■ EXPERIMENTAL SECTION

Molecular Models. Escin (Figure 1) is selected for this study because highly purified, single-molecular-species extracts are available and can be studied experimentally, which allows the construction of molecular models mimicking as close as possible the experimental conditions. In addition, escin is one of the saponins with the highest surface elasticity.[12,26,27]

To characterize the behavior of escin at the surface of water, MD simulations of four types of escin models are carried out (Figure 2): (1) a single nonionic surfactant; (2) a single anionic molecule, which is formed upon ionization of the carboxyl group present in one of the sugar residues, (3) 16 nonionized molecules, and (4) 16 anionic molecules.
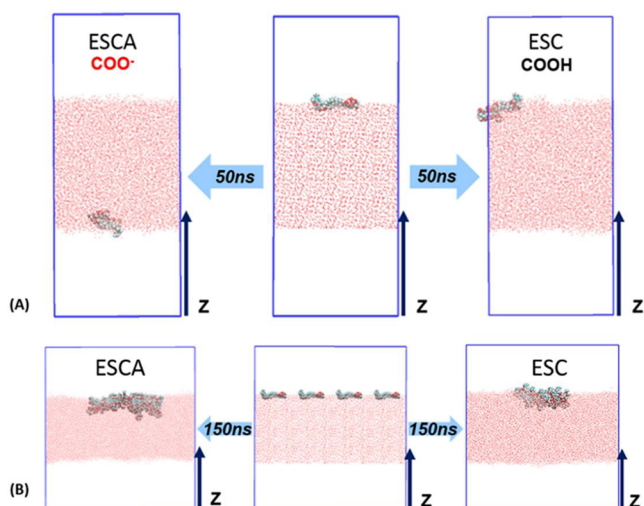
Figure 2. Simulated molecular models of (A) a single-surfactant and (B) 16 molecules at the vacuum−water interface. The initial configurations (middle) are shown together with the final snapshots from the MD simulations of neutral (right) and anionic (left) forms of escin molecules.

The initial geometry and the molecular mechanical parametrization of escin are described in the Supporting Information (Figures S1 and S2; Tables S1 and S2). In summary, the obtained atomic charges are

added to the AMBER99[22,23] force field, which is used to simulate escin in combination with model TIP3P[24] for the water molecules. Optimized geometry escin-1 (Figure S1) is taken as the starting structure for the atomistic MD simulations. In the first type of model, one neutral escin molecule is placed at the vacuum/water interface, its hydrophilic part being immersed within an ensemble of 12 326 explicit water molecules (Figure 2A). This model corresponds to a solution with a bulk concentration of 4.5 mM, where the molecule had adsorbed onto the air−water interface. The area per molecule in such a system would be 52 nm^2. In this model, the adsorbed escin molecules would not interact with each other. The model also contains 2 Na$^+$ and 2 Cl$^-$ ions to mimic the experimental conditions with 10 mM NaCl added to the solution. The periodic box sizes are x = 7.18 nm, y = 7.18 nm, and z = 17.18 nm. The second type of model system encompasses one escin anion and is built on the basis of its neutral counterpart by just removing the carboxylate proton (marked in bold in Figure 1A) and adding one more Na$^+$ as a neutralizing counterion.

The neutral and anionic models with 16 escin molecules (Figure 2B) also have identical starting configurations. They are built by translating the corresponding single-molecule model system into the XY plane, resulting in a regular initial spacing of the escin molecules at the surface. The sizes of the periodic boxes encompassing 16 hydrated escins are x = 16 nm, y = 6.4 nm, and z = 17.18 nm. In these larger models, the hydrophilic parts of the 16 surfactant molecules are immersed in a pool of 23 560 water molecules. The area per molecule in such an adsorption layer is 6.4 nm^2. This reproduces the conditions of a dilute adsorption layer; i.e., the model describes the initial stage of the adsorption experiments. Hence, the results presented in the current study should be regarded as the first step in unveiling the
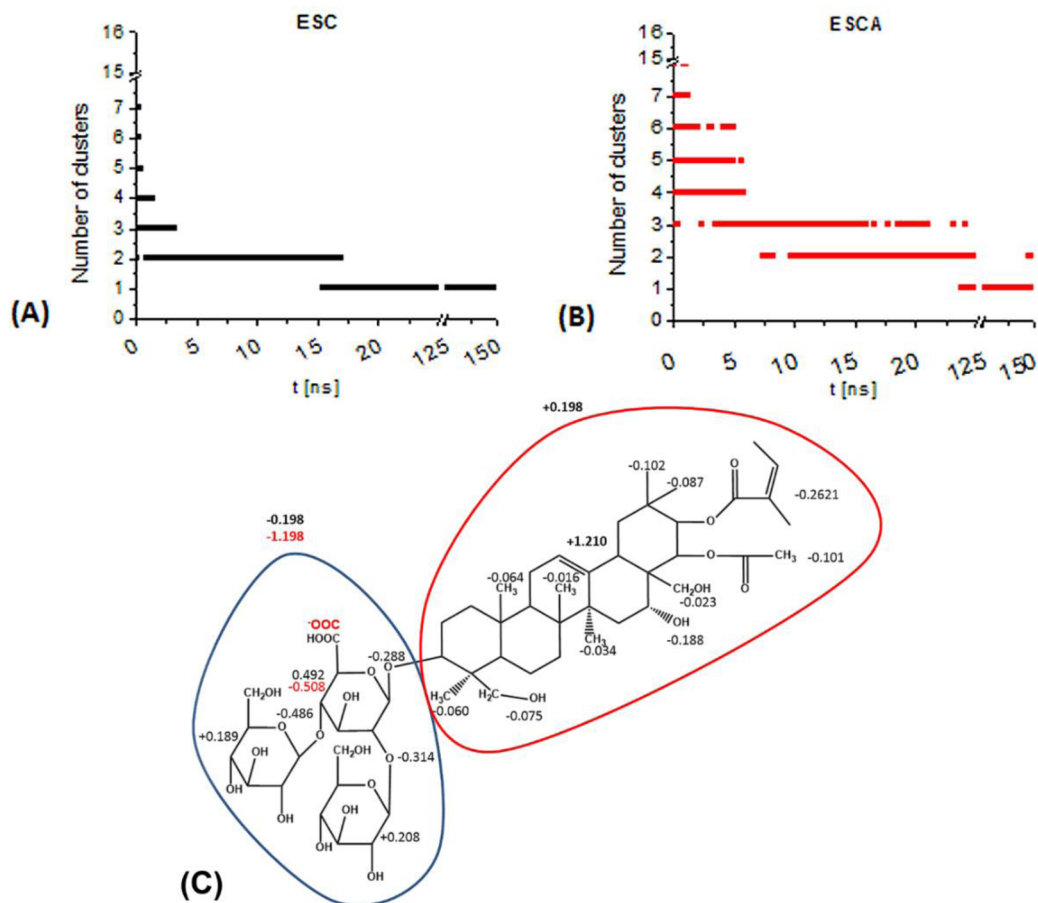

Figure 3. Evolution of the number of escin clusters in the 150 ns MD simulations of the 16-surfactant models of the (A) neutral and (B) ionized forms. (C) RESP group charges of the different molecular fragments of neutral and anionic escin. The values that do not coincide in the neutral and ionic forms are written in red.

surface characteristics of escin adsorption layers. The simulations of the 16-molecule models are also carried out in the presence of 10 mM NaCl, which corresponds to 4 Na$^+$ and 4 Cl$^-$ ions in the boxes. In the model with escin anions, an additional 16 Na$^+$ are present to neutralize the charge of the deprotonated carboxylic groups.

Computational Protocol. Periodic boundary conditions are applied in all simulations. A 5 nm vacuum space is included along the Z axis (which is normal to the interface) both above and below the water layer to create the water−vacuum interface (Figure 2). The MD runs are at constant temperature of 293 K maintained by a Berendsen thermostat.[25] The periodic box volume and the number of molecules are also fixed. These conditions and concentrations are chosen to mimic the experimental studies carried out by Pagureva et al.[12] and by Golemanov et al.[26,27]

The Lennard-Jones nonbonded potential is truncated at a cutoff distance of 1 nm with a switch function activated at 0.8 nm. Electrostatic interactions are evaluated in the monopole approximation with the PME method.[28−30] The direct part of the sum is truncated at 1.2 nm with a switch function turned on at 1 nm. The time step for the integration of the equations of motion is 2 fs, and the leapfrog algorithm is used. The lengths of all H-containing bonds are constrained with LINCS[31] in the surfactants and with SETTLE[32] in the water molecules.

A standard protocol is employed for the MD simulations—energy minimization, followed by heating and equilibration of the systems. The evolution of the energy and temperature is followed to verify that equilibrium has been reached. After that, production runs are generated with a length of 50 ns for the single-surfactant models and of 150 ns for the 16-surfactant systems. In all trajectories, the frames are recorded at intervals of 1 ps; i.e., the statistical analysis reported below encompasses 50 000 or 150 000 data points, respectively, unless otherwise specified.

To track the aggregation kinetics of escin in the 16-surfactant models, cluster analysis is performed with a limiting distance for a similarity of 0.028 nm. Only the coordinates of the escin molecules are included in this analysis.

The simulations of the single-surfactant models are carried out with Gromacs 4.5.2,[33] and those of the 16-surfactant ones, with Gromacs 4.6.5.[34] The VMD 1.9.1 package is used for visualization.[35]

■ RESULTS AND DISCUSSION

Surface Self-Assembly of Escin. It is revealing to trace first the trajectories of the molecules in the 16-surfactant models. The cluster analysis of the neutral surfactant model (Figure 3A) shows that at up to 3 ns various short-lived clusters are formed, with their number decreasing upon progress of the simulation. After 3 ns, only two stable clusters exist, each of them containing eight escin molecules. At ca. 17 ns, these clusters merge to yield a single 16-surfactant cluster, which remains stable until the end of the simulation at 150 ns. This is a very important outcome of our simulations because the spontaneous self-assembly of the adsorbed molecules indicates that strong, long-range attractive forces act between them. These forces lead to fast aggregation at the surface and prevent the formed cluster from breaking apart, which is in agreement with the experimentally registered fast formation of monolayers with high surface elasticity.[12,26]

Spontaneous self-assembly is also observed for anionic escin (Figure 3B). However, its molecules aggregate much more slowly compared to the neutral surfactant—a relatively stable 16-molecule cluster forms at 59 ns. Moreover, at up to 150 ns this cluster often breaks into two smaller clusters of 12 and 4 surfactant molecules, which then reassemble. This slower aggregation of the anionic form agrees qualitatively with the experimental finding that the energy of attraction between the adsorbed escin molecules is smaller in magnitude at pH 8 when the escin molecules are ionized as compared to that at pH 4

when the escin molecules are neutral (unpublished results). Figure 2B shows the final frames from the 150 ns simulations. It is evident that the surfactants are aggregated, leaving the larger part of the surface uncovered irrespective of the ionization state of escin.

The origin of the long-range attractive force driving cluster formation could be sought in the nonbonded interactions between the aglycone molecular fragments, which are not immersed in water. (See the next section for the relative position of these fragments with respect to the air−water interface.) To check this assumption, we calculated the group charges for the various parts of ESC and ESCA molecules (Figure 3C). As expected, the calculated group charges are unequally distributed along the escin molecules. The most negative charges belong to the oxygen-containing functional groups in the hydrophilic part of the molecule (immersed in water), but the residues comprising the carbon−carbon double bond, the hydroxyl group, and the acetate residue in the aglycone are also negatively charged. In other words, the entire molecular periphery is negatively charged, whereas the cyclic fragments in the aglycone center bear a significant positive charge (Figure 3C).

Such charge distribution implies the appearance of electrostatic attraction between the oppositely charged molecular fragments in the neighboring surfactant molecules when they are properly oriented with respect to each other. This attraction is a kind of dipole−dipole intermolecular interaction (more precisely, multipole−multipole interaction) and could explain the fast formation of the molecular clusters at the interface. This picture also implies that the molecules in the forming cluster should assemble in a preferred mutual orientation that maximizes this intermolecular attraction. In addition, upon closer approach of the aglycones, they interact via dispersion (London)-type attractive forces, which should be rather significant between such large molecular fragments. Rough estimates show that the total intermolecular energy between the neighboring aglycones could be well above $10kT$ (where kT is the thermal energy) if the aglycones are properly oriented with respect to each other.

For brevity, hereafter we denote the latter two types of forces (multipole−multipole and dispersion) as van der Waals forces between the aglycones. Note that the respective forces between the molecular fragments immersed in water are expected to be orders of magnitude smaller as a result of the high dielectric constant of the water medium (which decreases the multipole−multipole interactions in accordance with Coulomb's law) and the reduced Hamaker constant for interaction across the aqueous medium, as compared to the interaction across vacuum. Therefore, in the following discussion we consider the van der Waals interactions between the escin molecular fragments immersed in the aqueous phase in the initial stages of cluster formation to be negligible.

Expectedly, after deprotonation of the carboxyl group, the negative charge in the anionic ESCA molecules is localized mainly on the carboxylate anion, with part of the charge transferred to its adjacent cycle. (See the charges shown in red for ESCA in Figure 3C.) This results in a large negative charge on the hydrophilic part of the anion, which is immersed in water, whereas the aglycone part bears virtually the same distribution of charges as that in the neutral ESC. This comparison between ESC and ESCA shows that a long-range van der Waals attraction between the aglycones is expected for both types of molecules—neutral and ionized. However, it
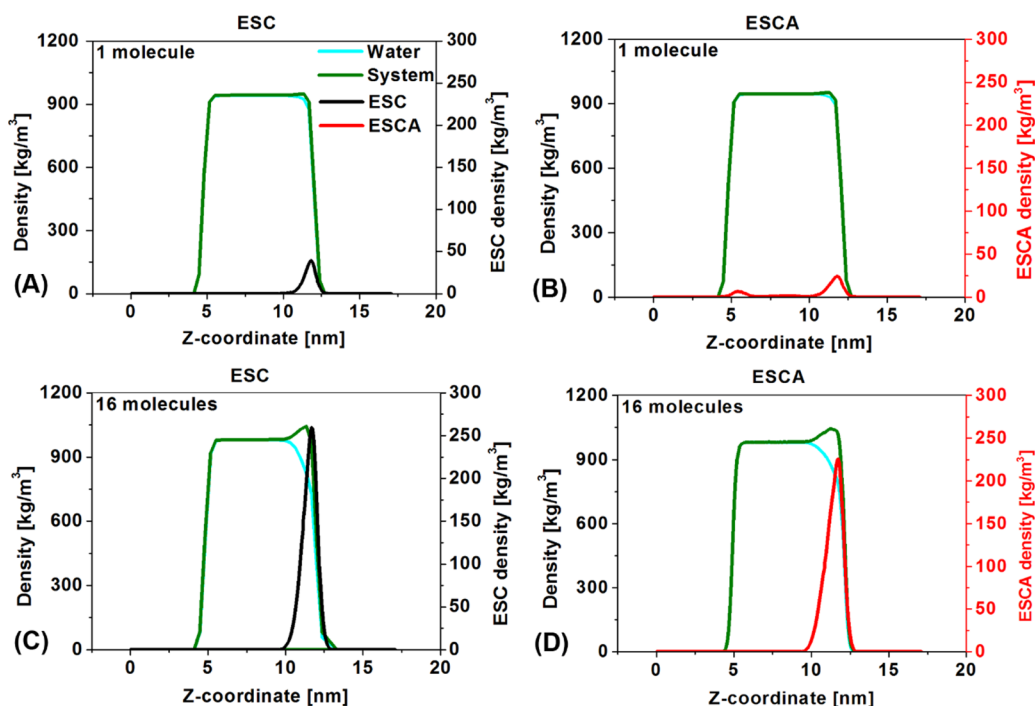
Figure 4. Density profiles in a direction normal to the interface for the entire system, water, and escin in the models of (A) single ESC, (B) single ESCA, (C) 16 ESC, and (D) 16 ESCA. The left ordinate is for the density of the system and water, and the right ordinate is for that of the surfactants.

would be superimposed over a long-range electrostatic repulsion between the charged hydrophilic fragments in the ESCA molecules. The electrostatic repulsion explains the two most important features in the evolution of the clusters of ionized ESCA molecules, namely, the slower aggregation kinetics and the lower stability of the largest cluster.

After the strong aggregation affinity of escin is revealed from the simulations, in the following sections we characterize the positions and orientation of the escin molecules with respect to the water surface and inside the clusters. The shorter-ranged interactions between the clustered escin molecules are also quantified. In the last section, we combine all of this information to explain the molecular processes observed in the simulations and discuss their possible relation to the experimental results for the rheological properties of escin adsorption layers.

Position of the Amphiphiles Relative to the Interface.
An analysis of the density profiles along the Z axis of the models provided the characteristic layer thicknesses in a direction normal to the interface. The mass densities of the whole systems, escin, and water (Figures 4 and S3) are calculated for all models by block averaging the production runs in 10 ns sections. This resulted in mean standard errors of the estimates of the escin density of 0.01 and 0.13 kg·m^{-3} for the small neutral and ionized models and of 0.06 and 0.04 kg·m^{-3} for the large models, respectively.

The following quantities are evaluated from the density profiles: (1) the most probable thickness of the escin cluster, as the full width at half maximum (fwhm) of the Gaussian fit of ESC/ESCA peaks, and (2) the maximum thickness of the escin cluster as the difference in the Z coordinates corresponding to the escin density at three standard deviations to the left and to the right from the Gaussian peak maximum. (For the sensitivity of the estimates to the position of fixing this minimum density, refer to Tables S3 and S4 of the Supporting Information.)

The density profiles of ESC and ESCA differ significantly. The peak of neutral escin is located close to one of the water surfaces (where the molecules were initially placed), irrespective of the model size (Figures 4 and S3, left), which is a clear indication of the high surface activity and low hydrophilicity of the neutral amphiphile. The same peak for the ionic form is shifted toward the interior of the aqueous layer (Figures 4 and S3, right), which shows that the anionic surfactant is immersed deeper into water. Moreover, in the single-molecule model of ESCA, a second density peak for the surfactant is present, mirroring the main one but at the opposite water surface (Figure 4, top right). This second peak is due to the dissolution of the ESCA molecule in the water, followed by transfer to the second interface, as confirmed by a visual inspection of the MD trajectory. This behavior outlines the anionic form of escin as being much more water-soluble, which is in agreement with the experimental results indicating that the anionic form of escin is more soluble than the neutral one.[13]

The most probable thickness (projection along the normal to the interface) of the single ESC molecule is 0.88 nm, and that of ESCA is 1.05 nm. The respective values for the 16-surfactant models are 1.08 nm for ESC and 1.27 nm for ESCA. As expected, these thicknesses are larger for the clusters. This increase can be due to thermal fluctuations of the molecules in the direction normal to the interface and/or to certain intermolecular interactions, which shift the individual molecules along the normal to the interface so that the escin molecules adjust their positions with respect to the neighboring ones. The latter effect is expected to be more pronounced in a cluster of charged molecules because it reduces the electrostatic repulsion between the neighboring molecules. ESCA is always thicker than ESC, irrespective of the model size, and this is in line with its higher hydrophilicity. The latter allows the molecules to
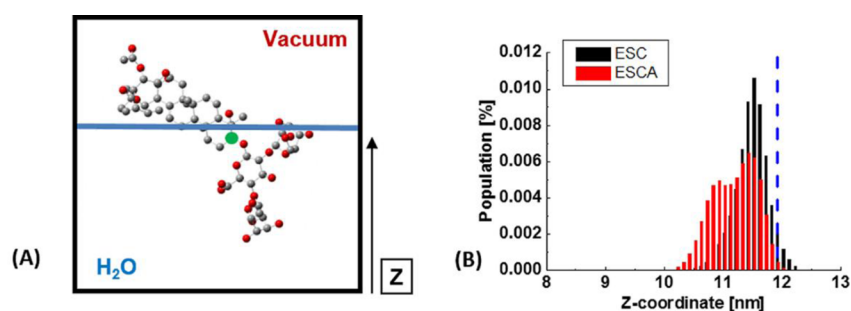
Figure 5. (A) Schematic representation of the selected reference aglycone carbon atom of escin and (B) distribution of its Z coordinate in the last 50 ns of the simulations of the 16-surfactant models; the blue dashed line denotes the equimolecular dividing surface for water.
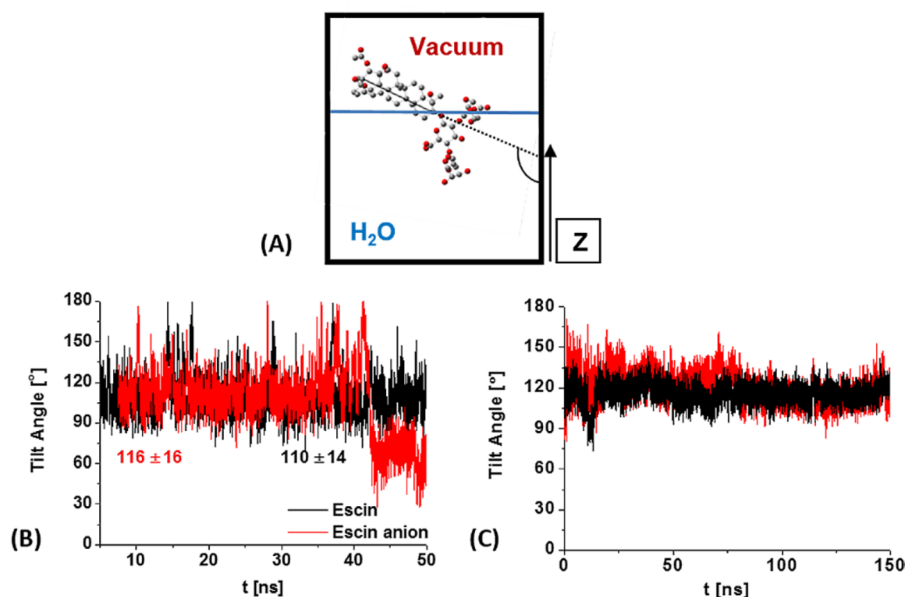

Figure 6. (A) Schematic presentation of the angle closed between the aglycone of escin and the Z axis and its evolution during the MD simulations of (B) the single-surfactant and (C) the 16-surfactant models.

submerge deeper into water and, hence, to occupy a broader interface region.

The maximum thickness (projection along the normal to the interface) of the surfactants in the normal direction is as follows: 2.24 nm for single ESC, 2.68 nm for single ESCA, 2.75 nm for the ESC cluster, and 3.24 nm for the ESCA cluster. Again, the anions are thicker. This is also an indirect reflection of the packing of the molecules in the cluster, which is looser for the anions than for the neutral surfactants. In addition, the thickness increases when going from the single- to the 16-molecules models, which points to fluctuations/shifts in the positions of the molecules along the Z axis in the clusters.

To check the latter assumption, additional analysis is performed. It uses a reference atom in the surfactant molecule, which marks the location of these molecules with respect to the interface. The Z coordinate of the terminal carbon atom in the aglycone, connecting it to the sugar residue (denoted in green in Figure 5A) is selected for this purpose. The reason is that the aglycone is relatively rigid and the position of this specific atom can be used to represent the vertical displacement of the entire aglycone.

The evolution of this Z coordinate for each of the 16 molecules in the cluster is recorded for the last 50 ns of the trajectories (Figure S4), and a summarized distribution is provided in Figure 5B. One sees that the Z coordinate

fluctuates on average in the range of 0.7 to 0.8 nm, with some molecules featuring the dispersion of the coordinate even above 1 nm. This result, combined with the significant width of the peaks in the histogram, confirms the assumed substantial mobility of the surfactants normal to the interface, which is especially pronounced for the anions. To quantify precisely the position of the aglycone with respect to the air−water interface, the equimolecular dividing surface for water (EDS, denoted in blue on Figure 5B) is determined as the Z coordinate in the density profile of water (Figure 4) corresponding to a water mass density of 500 kg/m^3. The Z coordinate of the reference escin atom is almost exclusively below the EDS, by ca. 0.5 to 1 nm. This means that the aglycone is partially immersed in water, which is in line with the known significant solubility of escin in water.[13]

The neutral and anionic forms differ in one more aspect. On one hand, the peak for the Z coordinates of ESCA is shifted toward the water phase, compared to that of ESC. This is in accordance with the analysis of the density profiles, which outlined ESCA as more hydrophilic. On the other hand, the distribution of ESC is unimodal, whereas that of ESCA is bimodal (Figure 5B). This signifies that the aglycone of the ionic form has two preferred locations with respect to the interface, which may stem from the attempt of the anions to reduce the electrostatic repulsion between the neighboring

molecules by displacing approximately half of them in the normal direction.

The molecular length of the two forms of escin is estimated from the single-surfactant models as another characteristic structural parameter (Figures S5 and S6). The data show that the neutral molecule is slightly longer (2.22 nm) than the charged one (2.11 nm) and that the length of the more stretched ESC molecule fluctuates in a narrower range. These lengths would coincide with the thickness of the escin layer if the surfactant molecules were perpendicularly aligned to the interface. However, the lengths of both the neutral and the charged forms are much larger than this thickness, which may happen if the amphiphile molecules are tilted with respect to the interface (Figure 6). Therefore, an evaluation of this tilt and some other characteristic angles is done next.

Interfacial Orientation and Intramolecular Conformation of the Surfactants. To assess the surface orientation of escin, the tilt of the aglycone (Figures 6A and S6), which is the most rigid part of the surfactant, is used. The tilt is evaluated as the angle closed between the Z axis and a vector interconnecting the two terminal carbon atoms of the aglycone cyclic part (Figure 6A). This angle is calculated for each frame of the MD trajectories, and the results are shown in Figure 6B,C.

The plot for single surfactant molecules in Figure 6B reveals that the angle is significantly smaller than 180°, i.e., the molecules are not perpendicular to the surface, which is in line with the results described in the previous section. The average value of the angle is similar for the two escin forms: 110° for ESC and 116° for ESCA, with both profiles featuring fluctuations of ca. ±15°. Rarely, both surfactants reach an angle of 180°, which corresponds to normal alignment relative to the surface. Much more frequently, the aglycones are oriented parallel to the interface, i.e., at angles close to 90°.

The behavior of the ionic form during the last 10 ns is interesting (Figure 6B). There, a seemingly drastic variation of the tilt is witnessed. This is actually due to the transfer of the anion to the opposite vacuum–water interface, as discussed above. A visual inspection of the trajectory shows that the change in the tilt to ca. 65° is just a reorientation of ESCA at the second interface and in fact corresponds to the same alignment of the hydrophobic fragment with respect to this second interface. The difference in the angle values comes from the reversal of the aglycone vector direction relative to the Z axis (65° = 180° − 115°).

The evolution of the angle for all molecules in the 16-surfactant models is similar. Therefore, an illustrative curve for just one of these molecules is presented in Figure 6C. The tilt of the amphiphiles in the cluster practically coincides with that of the single surfactants. Hence, it can be concluded that this is the preferred orientation of the aglycone with respect to the surface, irrespective of the presence of neighboring surfactant molecules. Angles close to 90° are also achieved in the cluster, although seldom with fluctuations of the angle similar to those in the single-surfactant systems. However, an angle of 180° is not populated in the cluster models. This is most probably due to the fact that if the molecules align perpendicular to the interface then their bulky sugar residues would unfavorably disturb the interaction with the neighboring surfactants because of steric hindrance. Hence, such an orientation does not occur, and this is the only effect on the tilt that stems from cluster formation.

The main conclusion from the tilt angle analysis is that the preferred orientation of the aglycone relative to the surface is a robust characteristic, which is not affected by the presence of neighbors or by ionization of the escin at the studied low surface coverage.

The orientation of the sugar residues with respect to the aglycone is also analyzed to provide a comprehensive description of the amphiphile intramolecular conformation. The results from this analysis are presented in the Supporting Information, Figure S7. In summary, one branch of the sugar residue closes an angle of ca. 160° with the aglycone, independent of the charge state. The second sugar–aglycone angle is smaller and fluctuates less when it is close to 120°, whereas it is more flexible when it is smaller than 120°. The hydrophilic part of the surfactant as a whole is rather mobile and undergoes spontaneous conformational changes on the studied nanosecond time scale.

Mutual Orientation of the Escin Molecules within the Clusters. The 16-surfactant systems also allow us to analyze the mutual orientation of the molecules in a cluster. The last 50 ns from the MD trajectories are used to quantify the mutual alignment of the amphiphiles because this orientation is already established in this last part of the simulations. The mutual organization of the neighboring surfactants therein is an indicator of the structure of escin surface domains/layers at low surface coverage. Therefore, the first step in the analysis is the identification of the closest-neighbor surfactants, which we denote as actual neighbors of each escin in the neutral and anionic clusters. (The procedure is described in the Supporting Information, Figure S8.)

Figure 7 shows a histogram of the distribution of the number of actual neighbors of ESC and ESCA. Significant differences
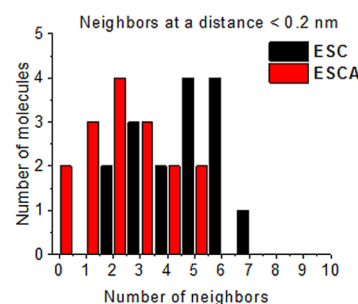

Figure 7. Number of neutral and anionic surfactants having a certain number of actual neighbors during the last 50 ns of the 16-surfactant simulations.

between the two systems are observed. The most frequent number of ESC actual neighbors is five or six, whereas that of ESCA is only two. The larger number of ESC neighbors indicates much better packing of the neutral molecules, stabilized by strong intermolecular attraction. In contrast, the small number of ESCA neighbors implies a looser packing, caused by the electrostatic repulsion between the ionized molecules.

The average separation of all possible surfactant pairs in the clusters is determined from an analysis of the minimum interatomic distance (the procedure is described in the Supporting Information, Figure S8), and the outcome is summarized in Table S5.

As can be seen, the number of ESC surfactant pairs at a distance of less than 0.2 nm is much larger than that of ESCA,

25 vs 13, which is in agreement with the larger number of actual neighbors for ESC (Figure 7). On the other hand, the number of pairs that changed their minimum distance to around 0.2 nm (i.e., those in which the surfactant molecules rearranged during the last 50 ns of simulation) is similar for ESC and ESCA (11 and 10, respectively). This shows that both the neutral and the charged surfactant molecules undergo some restructuring inside the clusters. The number of more remote surfactant pairs, which have an intermediate separation between 0.2 and 0.6 nm, is again much greater for ESC, 17 vs 6. These may be regarded as second neighbors indicative of liquid-type long-range ordering, which is present only in the neutral cluster. In contrast, there are many more remote pairs (separated by more than 0.6 nm) for the ionized surfactants, 91 vs 67, signifying the looser packing in the cluster of ESCA.

Hydration of the Escin Clusters by Water Molecules. The intra- and intersurfactant hydrogen bonds (H-bonds) within the neutral and ionized clusters are studied next to clarify the role of these bonds for the observed packing. The analysis of the entire clusters, also including the hydrogen bonding between escin and water, is given in the Supporting Information (Figures S9 and S10). It discloses that the number of escin−escin hydrogen bonds (H-bonds) increases during the MD simulations, whereas that of escin−water H-bonds decreases. The latter processes are slower in the anionic system. To explain this, it may be assumed that a larger number of water molecules protrude among the ionized surfactants to screen the electrostatic repulsion between the charged hydrophilic groups, thus also reducing the overall strength of interaction between the ESCA molecules. This would result in looser molecular packing and lower surface elasticity, in conjunction with the experimental findings.[12]

To verify the above hypothesis, an additional analysis is performed to determine the number of water molecules incorporated inside the surfactant clusters. For this purpose, the mass density profiles of water and escin in the normal direction are generated (Figure 8) for a subset of structures
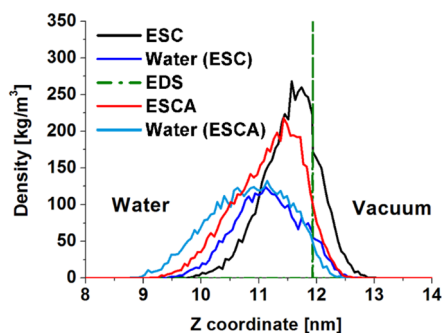

Figure 8. Mass density profiles of escin and water normal to the interface; the water profiles include only the water molecules located <0.4 nm from the escin molecules (first solvation shell). The averaging encompasses a set of 10 frames spaced at 5 ns, taken from the final 50 ns simulations of the neutral and ionized 16-surfactant systems.

(extracted at intervals of 5 ns from the last 50 ns of the MD trajectories), limiting the water profile to a distance of less than 0.4 nm from the surfactants, which corresponds to including the water molecules from the first solvation shell only.

The plot in Figure 8 shows that the density profile of ESC (black curve) is narrower than that of ESCA (red curve), which confirms the tighter packing of the neutral molecules.

Moreover, the peak of the anions is shifted toward water. Taking into account this shift and the position of the equimolecular dividing surface (EDS, the green line), the more strongly expressed hydrophilicity of ESCA is confirmed because a much smaller fraction of the anions can be found above the EDS, i.e., in the gas phase. The water profiles of the two systems are also different. The area encompassed by the dark-blue water curve (177 units), corresponding to the water present in the ESC cluster, is significantly smaller than that below the light-blue water curve from the ESCA system (239 units), which proves that there is much more water incorporated among the anionic surfactants, including also the space among the aglycones. This is corroborated by the larger number of water molecules (Table S6 in the SI) inside the anionic clusters, which confirms the presence of more hydrating water molecules.

Interactions between the Escin Molecules. The analysis of the total number of escin−escin hydrogen bonds (Figure S9) does not yield an unequivocal average number of hydrogen bonds per surfactant because the molecules have varying number of neighbors. Furthermore, most of the escin molecules are at the boundary of the clusters and hence do not form the maximum possible number of hydrogen bonds with their neighbors. From an experimental perspective, it can be expected that the elasticity of the escin layers would be related to the interactions between well-packed molecules, such as those in the core of the cluster. These reasons prompted us to perform a more in-depth analysis of the local hydrogen bonding of the actual neighboring escin−escin pairs in the cluster core.

The results for two representative molecular pairs of this type (one pair from the neutral system and one pair from the ionized one) are shown in Figure 9. A representative geometry of the two pairs is displayed in Figure 9A, showing that the two noncharged ESC molecules are very well packed whereas the aglycones of the two charged ESCA molecules are not aligned well with respect to each other. The two molecules in each pair have a minimum interatomic distance of close to 0.2 nm during the entire simulation, combined with a significant number of intermolecular contacts (especially for the ESC-ESC pair); i.e., they are actual permanent neighbors. The ESC molecules in the neutral pair have ∼5 actual neighbors per molecule on average. For the charge-paired ESCA molecules, the average number of neighbors is ∼1.5 per molecule.

One of the surfactants in the neutral pair forms more than 10 H-bonds on average with its 5 neighboring molecules, whereas the other surfactant forms fewer than 5 H-bonds with its 5 neighbors (Figure 9B, left). Most of these H-bonds are strong (Figure 9C, left), with a length of around 0.19 nm (Supporting Information). The H-bond length distribution of both molecules, however, contains an additional peak, centered at ca. 0.32 nm, that is especially intensive for one of the molecules in this pair. Such a characteristic length is too long to correspond to a typical H-bond. On the other hand, these forces exhibit a strong angular dependence, which is a characteristic feature of the H-bonds. Therefore, these longer-range attractive forces have a nature intermediate between that of classical H-bonds and the strong dipole−dipole interactions between the permanent dipoles of the interacting −OH groups in the molecules.[36] These H-bonds are formed when an appropriate steric match of the molecules is realized, which favors the proper orientation and the intermediate distance characterizing them.[36] They take place when the chemical structure of the particular molecules allows both appropriate
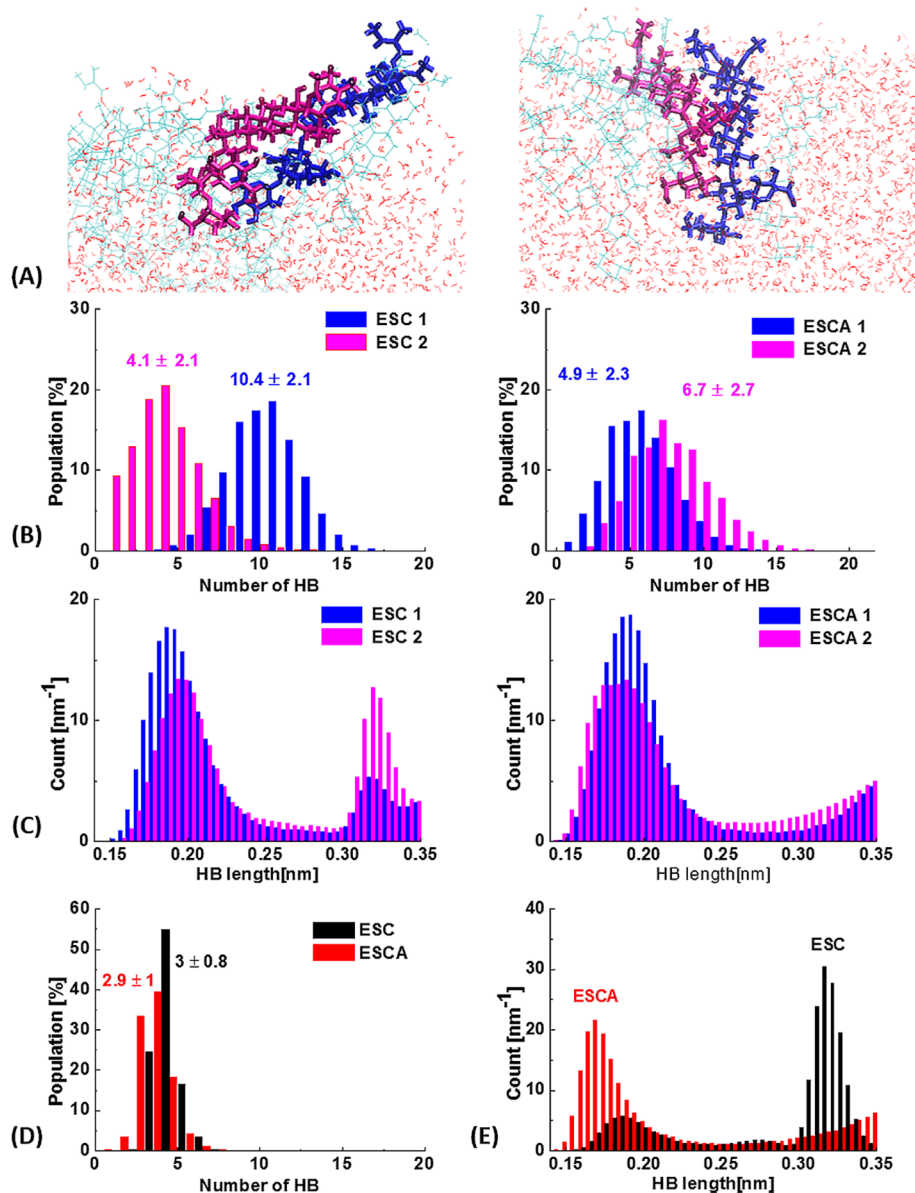
Figure 9. Analysis of the hydrogen bond distributions for well-packed molecules from the ESC and ESCA clusters. (A) Illustration of the molecular packing in the analyzed escin pairs. Distribution of the (B) number and (C) length of the escin−escin H-bonds of the two molecules from the pair with all of their actual neighbors. Distribution of the (D) number and (E) length of the H-bonds within the escin pairs only.

molecular packing and suitable orientation of the groups involved in these bonds.[36] For convenience, hereafter we call these forces either long-range H-bonds or specific dipole−dipole interactions, bearing in mind their intermediate nature.

These intermediate forces seem to play a role in the stabilization of the two neutral ESC molecules in the pair. One of the molecules orients its proton-accepting and proton-donating groups in such a way as to allow the formation of a maximum number of classical H-bonds with the other neighbors, whereas the second molecule in the pair maximizes these dipole−dipole interactions at the expense of the classical H-bonds. To check this hypothesis, the H-bonds between these two molecules are analyzed (Figure 9D,E). The data (the black columns) in Figure 9D show that ESC1 and ESC2 are connected by three H-bonds on average. Comparing this number to the one with all of their neighbors (Figure 9B), it becomes evident that unequal numbers of H-bonds are present between these two molecules and their neighbors. From the 10

H-bonds ESC1 forms with its neighbors, 3 are with ESC2 and the remaining 7 are with the other four neighbors. Respectively, from the total of four H-bonds of ESC2, three are with ESC1 and only one bond is with the other four neighbors. The bond length distribution of the three H-bonds formed between ESC1 and ESC2 (Figure 9E, black columns) is also nonstandard. The peak at 0.19 nm has lower intensity, whereas the peak representing the longer-range dipole−dipole attraction is very intensive. Thus, we conclude that this additional dipole−dipole attraction between the sugar residues of two neutral neighboring escin molecules stabilizes the pair, beside the classical short-range H-bonds.

A closer look at the simulated molecules showed that the latter H-bonds involve several hydroxyl groups in the two terminal sugar residues of the neighboring escin molecules (Figure S11). The two classical H-bonds involve the same terminal H atom in the −CH$_2$OH group of the ESC1 molecule (attached covalently to the O atom denoted by number 1 in

Figure 1B). At around 30% of the last 50 ns of the simulations, this H atom is involved in an H-bond with a mean distance of around 0.19 nm with an O atom number of 10 in the neighboring ESC2 molecule. The energy of the H-bonds of such a length is known to be in the range between 17 and 58 kJ/mol ($7kT$ to $22kT$ per bond).[36] Taking into account that this H-bond is active only around 30% of the time, one could estimate its contribution to the molecular pair stabilization to be between $2kT$ and $7kT$ (around $4.5kT$ on average). The same H atom was involved around 10% of the simulation time in another H-bond with O atom number 14, belonging to another −OH group in the sugar ring of ESC2. This gives an additional energy of attraction between the two molecules of $0.7kT$ to $2.2kT$ (around $1.5kT$ on average). It seems that this H atom flips between the two oxygen atoms in the neighboring ESC2 molecule by a minute conformational change in the −CH$_2$OH group to which it belongs. In total, these two H-bonds contribute ∼$6kT$ to the stabilization of this pair of escin molecules.

The third H-bond is formed at the H atom attached to O atom number 47 in ESC1 with O atom number 44 in the neighboring ESC2 molecule (Figure 1B). This bond distance is longer, ∼0.32 nm, but it is preserved for the entire period of the last 50 ns, which shows that it is unexpectedly stable. Taking into account that this interaction is of the dipole−dipole type and hence that it should decrease as r^3 (where r is the dipole−dipole distance), we can estimate this bond to be an order of magnitude weaker than the H-bonds described above. Averaged over time, this third H-bond should make an additional contribution to the molecular pair stabilization of $1kT$ to $2kT$. Note that this bond is formed between the other two terminal sugar residues in the neighboring escin molecules. Also, it may remain stable for a long time only if the interacting atoms are stabilized in the respective configuration by the overall packing of the ESC1 and ESC2 molecules; otherwise, this bond would be very labile and would live for less than 1 ns.

Similar analysis, performed for the closest neighboring pair of the ionized ESCA molecules (Figure 9D,E, red columns), led to different conclusions. The two anionic surfactants form around 6 ± 3 H-bonds with their actual neighbors (Figure 9B, right). On average, three of these bonds are between the two molecules in the close ESCA−ESCA pair, and the other three bonds are with molecules situated around this pair. The main H-bonds in the pair are realized between the H atoms attached to O atoms 44 and 47 (belonging to two neighboring hydroxyl groups in one of the terminal sugar residues) with the two oxygen atoms in the ionized carboxyl groups of the other ESCA molecule in the pair, viz., with O atoms 57 and 58. These H-bonds are particularly short, with a length of around 0.17 nm, which indicates that they are very strong, with an energy of around $20kT$ per bond.[36] Taking into account the fraction of the period in which these bonds are active (50, 40, 20, and 15% of the last 50 ns of the simulation, respectively), we can estimate that their contribution to the total interaction energy between the two paired ESCA molecules is significant, around $25kT$. Long-range dipole−dipole interactions, at ∼0.32 nm, are also realized between the ESCA molecules in the pair but much less than between the neutral surfactant molecules (Figure 9E), and their energy contribution is an order of magnitude lower. The H-bonds of the paired ESCA molecules with their neighbors are longer; therefore, the cohesive energy of the ESCA pair with their neighbors is relatively low. Furthermore, between the charged carboxyl groups, separated at around 1.2

nm in the ESCA pair, we have an additional electrostatic repulsion. It is difficult to estimate its energy because the relative dielectric constant, ε, around the charged carboxyl groups is not known and could be much lower than that of bulk water, $\varepsilon \approx 79$.[37] Approximate estimates by Coulomb's law, assuming $\varepsilon \approx 10$, show that the energy of electrostatic repulsion should be above $5kT$. In addition, as mentioned above, the aglycones of the two paired ESCA molecules are not aligned; they are not well packed and are immersed in water to a large extent, as compared to the neutral ESC molecules. All of these differences indicate a lower van der Waals attractive energy between the aglycones of the charged ESCA molecules.

Discussion: Relation between Intermolecular Forces and Surface Viscoelasticity. In this section, we dwell briefly on how the revealed interactions between the escin molecules could explain the high viscoelasticity of the escin adsorption layers. The performed analysis showed two very important features of the studied escin clusters. First, they are formed very rapidly, which is an indication of a relatively strong and long-range attraction between the adsorbed molecules. Second, three essential types of complementary intermolecular interactions have been identified.

The first type of interaction takes place between the aglycone parts of the molecules. Because of the specific arrangement of the distributed positive and negative charges along the aglycone, a long-range electrostatic attraction acts between the escin molecules and orients them with respect to each other. The tilt of the aglycone molecules relative to the water surface can further facilitate the appropriate mutual orientation of the positively and negatively charged fragments of the aglycone, as shown in Figure 10. (See also the simulated
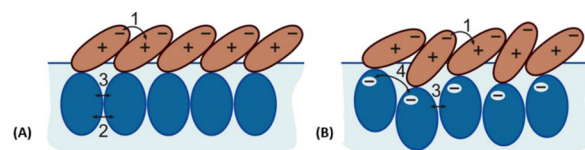

Figure 10. Schematic presentation of the arrangement of the escin molecules in a surface cluster for (A) neutral and (B) ionized molecules. The main intermolecular forces governing the escin self-assembly are (1) long-range attraction due to the inhomogeneous charge distribution in the aglycone and short-range dispersion (London) van der Waals forces between the aglycone fragments, (2) intermediate-range dipole−dipole/H-bond interaction, (3) short-range classical H-bonds, and (4) water-screened electrostatic repulsion between the charged carboxyl groups in the ionized escin molecules.

molecules in Figure 9A.) This attraction seems to be particularly pronounced for the noncharged ESC molecules, which are aligned very well with respect to each other.

For the ionic ESCA molecules, this long-range attraction is counteracted by the electrostatic repulsion between the charged carboxyl groups. The latter effect explains the slower kinetics of aggregation, the looser packing, and the larger fraction of water molecules inside the ESCA clusters (equivalent to the deeper immersion of ESCA molecules in the water phase). It also explains the observed two-peak distribution of the position of ESCA molecules normal to the interface (Figure 5B).

Inside the cluster of neutral escin molecules, preferred intermolecular distances corresponding to short-range (0.16 to 0.20 nm) and intermediate-range (0.30 to 0.35 nm) attractive H-bonds have been observed. Thus, we see that the clustering of the neutral molecules is governed by three complementary

types of attractive forces, which cover a wide range of intermolecular distances. At close-packing, all of these interactions combine in a synergistic way. The long-range van der Waals forces between the aglycones drive the molecule approach and orientation, whereas the intermediate and short-range H-bonds lock the molecular orientation and strengthen the attraction between the neighboring molecules. Note that all main fragments of the molecule, the aglycone, and the two terminal sugar residues are locked in the packed structure by the different types of interactions, explained above. See Figure 10 for an illustration of this conclusion. Therefore, increasing the intermolecular distance in the adsorption layer of neutral escin molecules would require the overcoming of all these forces (from very small to large distances), which could explain the observed high dilatational elasticity of the escin adsorption layers.[12]

Note that the relation between rheological properties and intermolecular interactions, including H-bonds, has been demonstrated qualitatively in other types of colloid systems. For example, in certain gels, formed by molecular self-assembly in solutions, the degree of viscoelastic recovery can be correlated qualitatively with the strength of H-bond interactions among the self-assembled molecules.[38]

Furthermore, the strong dependence of the H-bonds and of the intermediate dipole−dipole interactions on the mutual orientation of the molecules could also explain the relatively high shear elasticity of the escin adsorption layers.[12,27] The shear elasticity is further enhanced by the relatively rigid structure of the aglycone, which implies that any rearrangement of the closely packed molecules would be hindered by the limited flexibility of the aglycone scaffold.

The rearrangement of the molecules in sheared or dilated/compressed layers, at relatively large magnitudes of deformation, would require a series of bond-breaking and bond-forming events. These bond-breaking and -forming events lead to the dissipation of energy, which would be observed as a viscous response of the deforming adsorption layers. Thus, the intermolecular forces between the escin molecules, described in the current study, could explain the observed, excessively strong viscoelastic response of the escin adsorption layers.

Finally, most of the reported phenomena are registered for the ionic form of escin as well. However, they are less pronounced as a result of the strong electrostatic repulsion between the charged carboxyl groups in the hydrophilic part of the molecule. This repulsion precludes the fine packing of the charged ESCA molecules in a homogeneous layer, and thus, it explains the much lower surface elasticity, measured with the respective adsorption layers.[12]

CONCLUSIONS

Atomistic molecular dynamics simulations are carried out for escin (a representative of triterpenoid saponins) at the vacuum−water interface for both single and clustered surfactant molecules in neutral or anionic form. These simulations show that the escin molecules self-assemble very rapidly (for about 5 to 15 ns for the neutral form and within 60 ns for the anionic form), which indicates the presence of a strong, long-range attractive van der Waals forces between the aglycones of the adsorbed escin molecules. The aggregation kinetics of the ionic form is slower as a result of electrostatic repulsion between the hydrophilic molecular fragments of the ionized escin molecules. Eventually, both the neutral and anionic escin molecules form a single cluster at the water surface, which is much more compact

for the neutral form. Unlike the neutral escin molecules, the charged ones are loosely packed in the clusters and are displaced with respect to each other, in a direction normal to the interface, to reduce the intermolecular electrostatic repulsion.

The preferred tilt angle of the escin aglycones, relative to the interface, is around 115°. This angle is not affected by molecular ionization or by the presence of neighboring surfactant molecules in the cluster. The orientation of the sugar residues with respect to aglycone fluctuates a lot and spontaneous conformational transitions occur, which outline the significant flexibility of the sugar residues. Some molecules within the clusters are aligned with respect to each other, but regular ordering is not reached for the time of simulations (150 ns). The number of escin−escin hydrogen bonds varies significantly, depending on the intermolecular orientation. About three hydrogen bonds are formed on average between well-packed escin neighbors, irrespective of their charge. Between the neutral escin molecules, some of these bonds appear as specific attraction, intermediate in range and strength between the hydrogen bonding and dipole−dipole interaction.

ASSOCIATED CONTENT

Ⓢ Supporting Information

The Supporting Information is available free of charge on the ACS Publications website at DOI: 10.1021/acs.langmuir.7b01719.

> Initial structures of escin; atom numbering of the non-hydrogen atoms in neutral and ionized escin; rescaled density profiles of single molecules; Z coordinates of the terminal atom of aglycone; schematic picture of measured molecule lengths; length of molecules, hydrophilic or hydrophobic part; angles between aglycone and sugar chains; minimum distance and number of contacts for neighboring and non-neighboring molecules; number of inter- and intramolecular hydrogen bonds between escin molecules; number of intermolecular hydrogen bonds between escin and water molecules; representation of the hydrogen and oxygen atoms in the neighboring escin molecules between which H-bonds are formed; atomic connectivity information; RESP atomic charges; parameters from Gaussian fits of density profiles; thickness of escin; number of surfactant pairs found at different average minimum distances apart; number of water molecules ≤ 0.4 nm from escin molecules. (PDF)

AUTHOR INFORMATION

Corresponding Author
*E-mail: aivanova@chem.uni-sofia.bg. Tel: ++359-2-8161520.

ORCID Ⓘ
Anela Ivanova: 0000-0001-6220-7961

Notes
The authors declare no competing financial interest.

■ REFERENCES

(1) Sirtori, C. R. Aescin: pharmacology, pharmacokinetics, and therapeutic Profile. *Pharmacol. Res.* **2001**, *44*, 183−193.

(2) Miyakoshi, M.; Tamura, Y.; Masuda, H.; Mizutani, K.; Tanaka, O.; Ikeda, T.; Ohtani, K.; Kasai, R.; Yamasaki, K. Antiyeast steroidal saponins from Yucca schidigera (Mohave yucca), a new anti-food deteriorating agent. *J. Nat. Prod.* **2000**, *63*, 332−338.

(3) Oakenfull, D. Soy protein, saponins and plasma cholesterol. *J. Nutr.* **2001**, *131*, 2971−2972.

(4) Shin, H. R.; Kim, J. Y.; Yun, T. K.; Morgan, G.; Vainio, H. The cancer-preventive potential of Panax ginseng: a review of human and experimental evidence. *Cancer Causes Control* **2000**, *11*, 565−576.

(5) Kensil, C. R.; Mo, A. X.; Truneh, A. Current vaccine adjuvants: an overview of a diverse class. *Front. Biosci., Landmark Ed.* **2004**, *9*, 2972−2988.

(6) Wang, Z. W.; Gu, M. Y.; Li, G. Z. Surface Properties of Gleditsia Saponin and Synergisms of Its Binary System. *J. Dispersion Sci. Technol.* **2005**, *26*, 341−347.

(7) Sarnthein-Graf, C.; La Mesa, C. Association of saponins in water and water−gelatine mixtures. *Thermochim. Acta* **2004**, *418*, 79−84.

(8) Mitra, S.; Dungan, S. R. Micellar properties of Quillaja saponin. 1. Effects of temperature, salt, and pH on solution properties. *J. Agric. Food Chem.* **1997**, *45*, 1587−1595.

(9) Mitra, S.; Dungan, S. R. Micellar properties of quillaja saponin. 2. Effect of solubilized cholesterol on solution properties. *Colloids Surf., B* **2000**, *17*, 117−133.

(10) Mitra, S.; Dungan, S. R. Cholesterol solubilization in aqueous micellar solutions of quillaja saponin, bile salts, or nonionic surfactants. *J. Agric. Food Chem.* **2001**, *49*, 384−394.

(11) Ibanoglu, E.; Ibanoglu, S. Foaming behaviour of liquorice (Glycyrrhiza glabra) extract. *Food Chem.* **2000**, *70*, 333−336.

(12) Pagureva, N.; Tcholakova, S.; Golemanov, K.; Denkov, N. D.; Pelan, E.; Stoyanov, S. D. Surface properties of adsorption layers formed from triterpenoid and steroid saponins. *Colloids Surf., A* **2016**, *491*, 18−28.

(13) Tcholakova, S.; Mustan, F.; Pagureva, N.; Golemanov, K.; Denkov, N. D.; Pelan, E.; Stoyanov, S. D. Role of surface properties for kinetics of Ostwald ripening in saponin stabilized foams. *Colloids Surf., A* **2017**, DOI: 10.1016/j.colsurfa.2017.04.055 http://www.sciencedirect.com/science/article/pii/S0927775717303874.

(14) Dudek-Makuch, M.; Studzińska-Sroka, E. Horse chestnut − efficacy and safety in chronic venous insufficiency: an overview. *Rev. Bras. Farmacogn.* **2015**, *25*, 533−541.

(15) Wei, F.; Ma, L. Y.; Cheng, X. L.; Lin, R. C.; Jin, W. T.; Khan, I. A.; Lu, J. Preparative HPLC for Purification of Four Isomeric Bioactive Saponins from the Seeds of Aesculus chinensis. *J. Liq. Chromatogr. Relat. Technol.* **2005**, *28*, 763−773.

(16) Pedebos, C.; Pol-Fachin, L.; Verli, H. Unrestrained conformational characterization of stenocereus eruca saponins in aqueous and nonaqueous solvents. *J. Nat. Prod.* **2012**, *75*, 1196−1200.

(17) Pedebos, C.; Pol-Fachin, L.; Pons, R.; Teixeira, C. V.; Verli, H. Atomic model and micelle dynamics of QS-21 saponin. *Molecules* **2014**, *19*, 3744−3760.

(18) Dai, X.; Shi, X.; Wang, Y.; Qiao, Y. Solubilization of saikosaponin a by ginsenoside Ro biosurfactant in aqueous solution: Mesoscopic simulation. *J. Colloid Interface Sci.* **2012**, *384*, 73−80.

(19) Walkowicz, W. E.; Fernandez-Tejada, A.; George, C.; Corzana, F.; Jimenez-Barbero, J.; Ragupathi, G.; Tan, D. S.; Gin, D. Y. Quillaja saponin variants with central glycosidic linkage modifications exhibit distinct conformations and adjuvant activities. *Chem. Sci.* **2016**, *7*, 2371−2380.

(20) Lin, F.; Wang, R. Hemolytic mechanism of dioscin proposed by molecular dynamics simulations. *J. Mol. Model.* **2010**, *16*, 107−118.

(21) Wu, D.; Feng, Y.; Xu, G.; Chen, Y.; Cao, X.; Li, Y. Dilational rheological properties of gemini surfactant 1,2-ethane bis(dimethyl dodecyl ammonium bromide) at air/water interface. *Colloids Surf., A* **2007**, *299*, 117−123.

(22) Cornell, W. D.; Cieplak, P.; Bayly, C. I.; Gould, I. R.; Merz, K. M., Jr.; Ferguson, D. M.; Spellmeyer, D. C.; Fox, T.; Caldwell, J. W.; Kollman, P. A. A Second Generation Force Field for the Simulation of Proteins, Nucleic Acids, and Organic Molecules. *J. Am. Chem. Soc.* **1995**, *117*, 5179−5197.

(23) Wang, J.; Cieplak, P.; Kollman, P. A. How well does a restrained electrostatic potential (RESP) model perform in calculating conformational energies of organic and biological molecules? *J. Comput. Chem.* **2000**, *21*, 1049−1074.

(24) Jorgensen, W. L.; Chandrasekhar, J.; Madura, J. D.; Impey, R. W.; Klein, M. L. Comparison of Simple Potential Functions for Simulating Liquid Water. *J. Chem. Phys.* **1983**, *79*, 926−935.

(25) Berendsen, H. J. C.; Postma, J. P. M.; van Gunsteren, W. F.; DiNola, A.; Haak, J. R. Molecular dynamics with coupling to an external bath. *J. Chem. Phys.* **1984**, *81*, 3684−3691.

(26) Golemanov, K.; Tcholakova, S.; Denkov, N. D.; Pelan, E.; Stoyanov, S. D. Remarkably high surface visco-elasticity of adsorption layers of triterpenoid saponins. *Soft Matter* **2013**, *9*, 5738−5752.

(27) Golemanov, K.; Tcholakova, S.; Denkov, N. D.; Pelan, E.; Stoyanov, S. D. The role of the hydrophobic phase in the unique rheological properties of saponin adsorption layers. *Soft Matter* **2014**, *10*, 7034−7044.

(28) Darden, T.; York, D.; Pedersen, L. Particle mesh Ewald: An N·log(N) method for Ewald sums in large systems. *J. Chem. Phys.* **1993**, *98*, 10089−10092.

(29) Essmann, U.; Perera, L.; Berkowitz, M. L.; Darden, T.; Lee, H.; Pedersen, L. G. A smooth particle mesh Ewald method. *J. Chem. Phys.* **1995**, *103*, 8577−8593.

(30) Toukmaji, A.; Sagui, C.; Board, J.; Darden, T. Efficient PME-based approach to fixed and induced dipolar interactions. *J. Chem. Phys.* **2000**, *113*, 10913−10927.

(31) Ryckaert, J.-P.; Ciccotti, G.; Berendsen, H. J. C. Numerical integration of the cartesian equations of motion of a system with constraints: molecular dynamics of n-alkanes. *J. Comput. Phys.* **1977**, *23*, 327−341.

(32) Miyamoto, S.; Kollman, P. A. Settle: An analytical version of the SHAKE and RATTLE algorithm for rigid water models. *J. Comput. Chem.* **1992**, *13*, 952−962.

(33) van der Spoel, D.; Lindahl, E.; Hess, B.; Groenhof, G.; Mark, A. E.; Berendsen, H. J. C. GROMACS: fast, flexible, and free. *J. Comput. Chem.* **2005**, *26*, 1701−1718.

(34) Hess, B.; Kutzner, C.; van der Spoel, D.; Lindahl, E. Gromacs 4: Algorithms for Highly Efficient, Load-Balanced, and Scalable Molecular Simulation. *J. Chem. Theory Comput.* **2008**, *4*, 435−447.

(35) Humphrey, W.; Dalke, A.; Schulten, K. VMD: Visual molecular dynamics. *J. Mol. Graphics* **1996**, *14*, 33−38.

(36) Jeffrey, G. A. *An Introduction to Hydrogen Bonding*; Oxford University Press: New York, 1997.

(37) Israelachvili, J. N. *Intermolecular and Surface Forces*, 3rd ed.; Academic Press: Amsterdam, 2011.

(38) Zhang, Y.; Weiss, R. G. How do H-bonding interactions control viscoelasticity and thixotropy of molecular gels? Insights from mono-, di- and tri-hydroxymethylated alkanamide gelators. *J. Colloid Interface Sci.* **2017**, *486*, 359−371.